C. R. Chimie 22 (2019) 621–627

Contents lists available at ScienceDirect

Comptes Rendus Chimie

www.sciencedirect.com

Full paper / Mémoire

Montmorillonite-stabilized gold nanoparticles for nitrophenol reduction

Meriem Chenouf [a, b], Cristina Megías-Sayago [a, *], Fatima Ammari [b], Svetlana Ivanova [a], Miguel Ángel Centeno [a], José Antonio Odriozola [a]

[a] Departamento de Química Inorgánica e Instituto de Ciencia de Materiales de Sevilla, Avda. Americo Vespucio 49, 41092 Sevilla, Spain
[b] LGPC, Department of Chemical Process Engineering, Ferhat-Abbas Sétif-1 University, 19000 Sétif 1, Algeria

ARTICLE INFO

Article history:
Received 20 May 2019
Accepted 16 July 2019
Available online 29 August 2019

Keywords:
4-Nitrophenol reduction
Gold nanoparticles
Montmorillonite
CeO_2

ABSTRACT

Two gold-based catalysts were obtained by Au chemical reduction of the $HAuCl_4$ precursor. The resulting nanoparticles were stabilized and immobilized on montmorillonite (Mt) and montmorillonite-ceria (Mt/CeO_2). All prepared catalysts were active in 4-nitrophenol to aminophenol reduction at room temperature. Synergy between montmorillonite and ceria is postulated in such a way that the montmorillonite phase hinders particle growth either by influencing the nucleation behavior of gold or by increasing the number of nucleation sites and raising the overall dispersion. The role of the ceria support, on the other hand, may be associated with the 4-NP adsorption at the ceria-gold interface, stabilizing the reaction intermediate and hence lowering the activation barrier for the reduction of 4-NP to 4-AP.

1. Introduction

4-Nitrophenol (4-NP) is one of the most widely used nitroaromatic compounds being found as a pollutant in surface and ground waters since its extensive use for dyes, pesticides, and pharmaceuticals [1–4]. When released into the environment, it can result in environmental and health risk because of its acute toxicity and mutagenic potential. As an example, concentration as low as ~5 $\mu g \cdot L^{-1}$ was set as the chronic toxicity level for saltwater aquatic fish [5]. To remove this pollutant, many processes have specifically been developed, microbial [6] or photocatalytic [7] degradation, adsorption [8], microwave-assisted catalytic oxidation [9], electro-Fenton method [10], or electrochemical treatments [11], among others. Within the different alternatives, the catalytic conversion of 4-NP to 4-aminophenol (4-AP) seems to be the most promising route to remove this pollutant. Indeed, 4-AP is a very important chemical in the pharmaceutical industry for the preparation of antipyretic and analgesic drugs, at the same time being less toxic than 4-NP [12]. This latter approach entails not only 4-NP elimination but also its valorization, which makes this method more suitable in comparison to those involving 4-NP degradation/oxidation, usually producing CO_2. The synthesis of 4-AP from 4-NP can be achieved via catalytic hydrogenation in ethanol at relatively high temperature and high hydrogen pressure [13,14]. However, operating at milder temperatures and avoiding the use of organic solvents would be extremely desirable to transition the overall process to safer and environmentally suitable conditions. Moreover, this technology may be also applied to wastewater-containing 4-NP to remove it [15].

Several noble metal nanoparticles, including silver, palladium, platinum [16–18], and gold [19–23], have been reported as effective in the catalytic reduction of 4-NP by $NaBH_4$. Among them, the best performances are observed when gold is used as the catalyst. In general, the apparent activity of the gold nanoparticles depends on their size and morphology, the nature of the capping

* Corresponding author.
E-mail address: cristina.megias@icmse.csic.es (C. Megías-Sayago).

https://doi.org/10.1016/j.crci.2019.07.005
1631-0748/

agent, and/or the presence of a mineral stabilizer (support). Several methods may be used for preparing monodisperse gold nanoparticles. These are divided into two main groups, precipitation and colloidal methods. In the latter, the use of a stabilizer during particle formation is mandatory to prevent excessive aggregation. For that purpose, surfactants [24] and/or polymers [25,26] are usually used. However, the use of stabilizers introduces bulky molecules that remain bound to the metal nanoparticles, which may be displaced by reactants and/or products or adsorbed on the nanoparticles blocking surface sites or even react with reactants and/or products. The removal of these capping agents is not an easy task, and its presence may strongly affect the apparent activity of the catalysts. In fact, it has been reported that catalyst self-conditioning occurs before reaction, *i.e.*, the capping agent is displaced by the substrates [27]. The rate of substrate adsorption is directly related to the metal/capping agent interaction; the stronger the interaction, the more difficult the substrate adsorption, resulting in the appearance of an induction period.

Alternatively, the immobilization of preformed colloids on high-specific-surface-area mineral supports [28–30] results in clean and well-dispersed gold nanoparticles. The use of clay minerals raises special interest as they are environmentally benign, costless, and abundant. Clays are demonstrated to be versatile materials that can be used as gold nanoparticle supports [31–34] and also as nanoparticle-stabilizing agents [35,36]. They are widely used as sorbents [37,38] and in catalysis for glycerol dehydration [31] or aromatic hydrocarbons production [32].

In this study, montmorillonite is used as a stabilizer and support of gold nanoparticles. The catalytic activity of the montmorillonite-stabilized gold nanoparticles in the reduction of 4-NP by $NaBH_4$ is analyzed. To discern its role as support and stabilizer, two different samples were considered: gold nanoparticles on montmorillonite and gold nanoparticles stabilized with montmorillonite and supported on commercial ceria support.

2. Experimental

2.1. Synthesis

2.1.1. Montmorillonite preparation

The natural bentonite was extracted from the Roussel deposit of Maghnia (Algeria). The first step was bentonite purification, aiming to remove sand feldspar and calcite impurities. For that, 10 g of bentonite was dispersed in distilled water (1 L) for 3 h and allowed to sediment for 24 h. Afterward, the uppermost two-thirds of the supernatant was separated, dried overnight at 80 °C, and sieved (100–200 μm mesh). Before use, the purified bentonite, mainly montmorillonite, was transformed to its homoionic Na-exchanged form using 1 M sodium chloride solution. The resulting powder was thoroughly washed and centrifuged several times, and just the <2 μm fraction of the Na-montmorillonite was retained. After this treatment, the sample was labeled Mt.

2.1.2. Montmorillonite-stabilized gold nanoparticle preparation

A 2 wt% Au nanoparticle montmorillonite-stabilized catalyst was prepared by chemical reduction of the corresponding gold precursor. An adequate amount of a $1*10^{-3}$ M $HAuCl_4$ (Alfa Aesar) was added to 10 ml of $NaBH_4$ aqueous solution (0.1 M) in the presence of 0.5 g of finely dispersed montmorillonite (Mt). After 1 h of vigorous stirring, the sample was centrifuged, washed, and finally dried overnight at 60 °C. This sample was labeled as Au–Mt. For comparative purposes, a ceria-supported catalyst was prepared following the same protocol (Au/CeO_2).

2.1.3. Montmorillonite-stabilized gold nanoparticles supported on ceria

Gold nanoparticles were prepared by chemical reduction of the $HAuCl_4$ precursor ($1*10^{-3}$ M) with $NaBH_4$ (0.1 M) in the presence of montmorillonite (Mt, 0.1 g) as stabilizer. Then, the colloid was mixed with CeO_2, followed by dispersion in distilled water at pH lower than its isoelectric point (4.8). The pH was adjusted using 0.1 M HCl. The sample was separated by centrifugation and labeled as $Au–Mt/CeO_2$ after washing and drying at 60 °C.

2.2. Catalytic reduction of 4-NP

Liquid-phase 4-NP reduction was carried out at room temperature. A 0.5:100:10,000 M ratio was set for the Au:4-NP:$NaBH_4$ mixture in all the experiments. Typically, 10 mL of $NaBH_4$ (1 M) aqueous solution was mixed with 10 mg of the catalyst previously suspended in distilled water. At t_0, 10 mL of an aqueous solution of 4-NP (10^{-2} M) was added, and the reaction time was initiated. The reaction rates may be taken as independent of the reductor concentration as the great excess of $NaBH_4$ and therefore a pseudo-first-order reaction can be considered [20].

The reduction process was monitored by UV-vis absorption spectrometry. Every 60 s, 1 mL of the reaction suspension was filtered and analyzed. Quantification was performed by integration of the bands at center at 398 nm belonging to 4-NP and at 298 nm ascribed to 4-AP.

2.3. Characterization

Brunauer–Emmett–Teller (BET) specific surface area and pore diameter, calculated by the Barrett-Joyner-Halenda (BJH) method, were measured by nitrogen adsorption at liquid nitrogen temperature in Micromeritics Tristar II equipment. The samples were outgassed before analysis at 250 °C in vacuum. UV-vis absorption spectra were recorded on a UV-vis Avantes AvaLight-DH-S-Bal equipped with an optic fiber liquid sensor for wavelengths ranged from 100 to 1000 nm. Gold contents of the catalysts were determined by X-ray fluorescence (XRF) using a Panalytical AXIOS spectrometer with Rh tube of radiation.

X-ray diffraction analyses were performed in the 5-80° 2θ range with 0.01° step size and 300 s step time on X'Pert Pro PANanalytical instrument using CuKα radiation.

Transmission electron microscopy (TEM) observations were carried out on TOPCON-002B microscope. Before analysis, all samples were dispersed in ethanol and

Table 1
Textural properties and gold loadings of the studied catalysts.

Samples	Au (wt %)	BET (m^2/g)	Pore size (nm)	Pore volume (cm^3/g)
Mt	–	56	8.5	0.08
Au–Mt	1.3	7	14	0.05
CeO_2	–	137	6.5	0.23
Au/CeO_2	2.3	137	6.3	0.24
$Au–Mt/CeO_2$	1.5	128	6	0.21

deposited on a holey carbon copper grid. The particle size distribution was estimated over 30 micrographs, and the mean gold particle diameter was considered based on its homogeneity and frequency of abundance over an important number of particles (typically >200). The mean gold particle size was estimated through Eq. 1.

$$D[3,2] = \frac{\sum_1^n D_i^3 v_i}{\sum_1^n D_i^2 v_i} \quad (1)$$

where D_i is the geometric diameter of the i^{th} particle and v_i the number of particles with this diameter.

3. Results and discussion

Specific surface areas, gold mean particle size, and gold content of the catalysts are reported in Table 1.

Upon gold addition, the surface area of the montmorillonite collapses, the total pore volume decreases, and the average pore size increases. On the contrary, the mesoporous ceria–containing catalysts hardly modify the textural properties of the bare ceria support. Moreover, the ceria-containing catalysts present much higher surface areas than the Au–Mt one. The amount of gold loading is a function of the support nature, with experimental values closer to the target ones for all ceria containig solids: in the case of the Mt-stabilized gold nanoparticles, the loading efficiency decreases by ~30%.

Fig. 1 presents the diffraction pattern of all the studied samples. The interlayer distance (d_{001}) of the montmorillonite samples (Fig. 1A) is quite close to those previously reported for other Na forms [39]. However, the irregular profile of the basal diffraction suggests the presence of different cations in the sample due to incomplete Na exchange and the presence of protons. The diffraction pattern remains unaltered upon gold loading. The typical gold diffraction line at 38° is not clearly observed, suggesting a very small particle size for gold; however, the complex diffraction pattern of the montmorillonite sample with a collection of overlapping diffractions prevents any further conclusion.

The diffraction patterns of all ceria-containing solids are characteristic of the F-type crystalline structure of CeO_2 (fluorite structure). Diffraction lines corresponding to montmorillonite or gold phases are not clearly observed. However, a slight broadening at *ca.* $2\theta = 38°$ in the Au/CeO_2 sample could suggest slightly bigger gold nanoparticles in the Au/CeO_2 catalyst than in the ones containing montmorillonite.

Although the contrast between gold and ceria phase, when present, is low, TEM allows us to estimate distribution and mean gold particle size (Fig. 2).

The estimated mean particle size for both Au–Mt and Au/CeO_2 catalysts is the same (5.5 and 5.6 nm, respectively). However, major differences can be observed in the particle size distribution of these catalysts. The Au/CeO_2 sample present an almost normal broad distribution centered at ~4 nm, while a logarithmic distribution decreasing from 1 to 10 nm is observed for the Au–Mt one. Despite the broad distributions, it seems that montmorillonite allows lower particle sizes. This suggestion is reinforced by considering the low contrast between gold and ceria phase that could also imply the underestimation of the mean particle size for the Au/CeO_2 catalyst as the smaller particles are easier to identify. This observed particle size sequence is in accordance to XRD data that may allow the observation of a gold diffraction line only for the Au/CeO_2 sample.

When both solids (Mt and CeO_2) are present in the catalyst ($Au–Mt/CeO_2$), the mean particle size is the smallest (4.1 nm). The particle size distribution for the $Au–Mt/CeO_2$ is the narrowest among the studied samples;

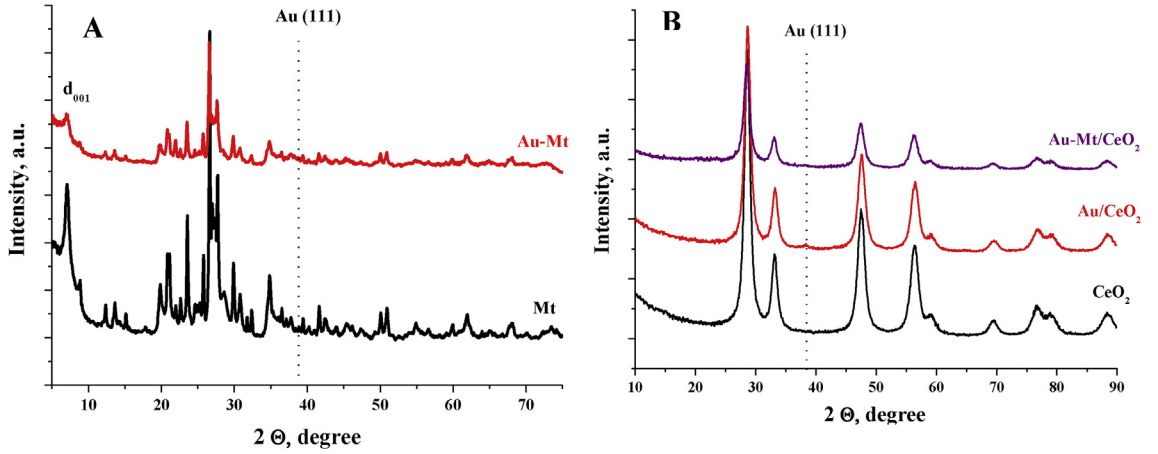

Fig. 1. XRD patterns of (A) Mt and Au–Mt samples and (B) ceria-based samples. XRD, X-ray diffraction.

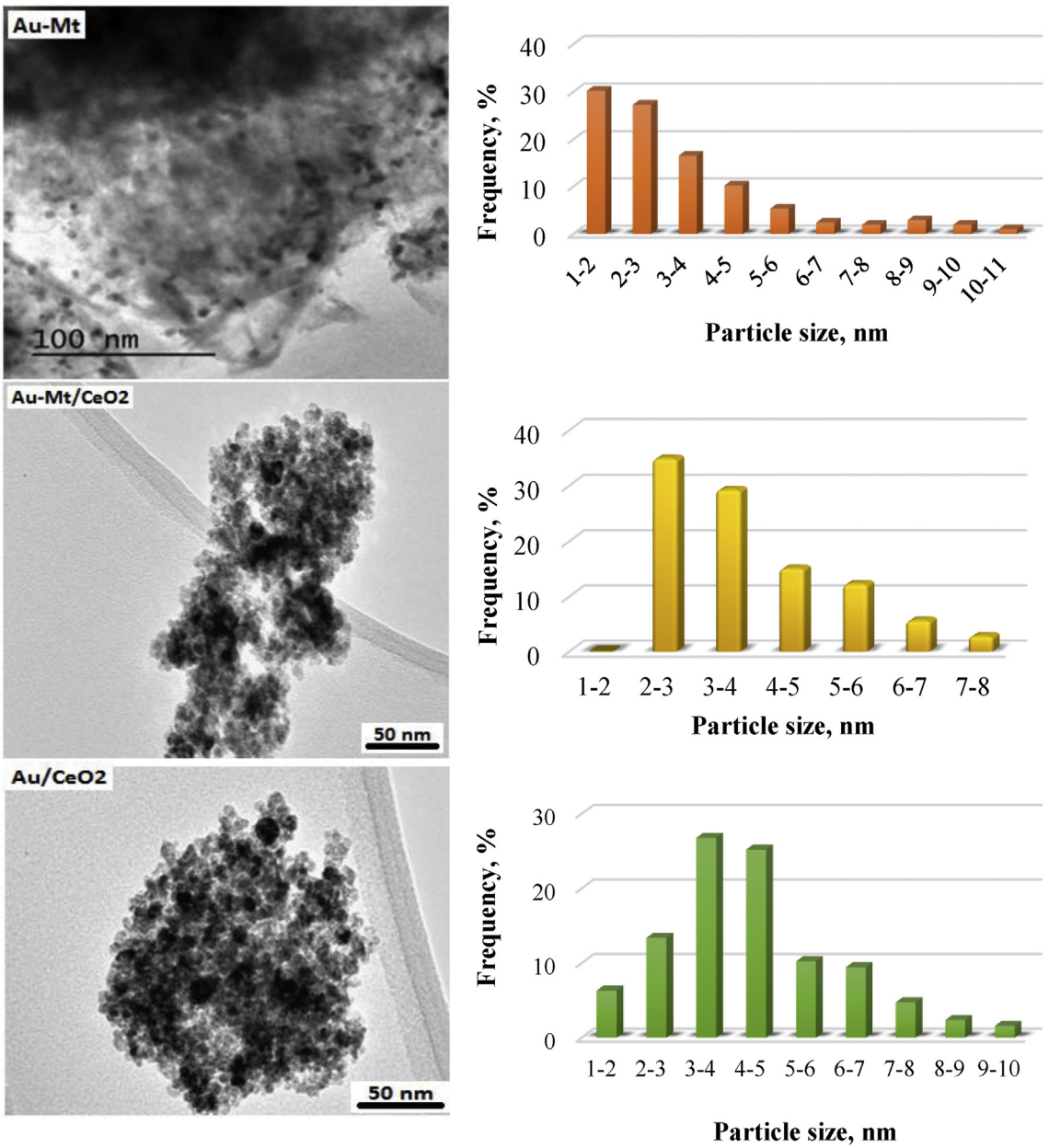

Fig. 2. Selected TEM images of the samples and their corresponding particle size distributions. TEM, transmission electron microscopy.

it follows the logarithmic trend observed for the Au–Mt sample but shifted to higher values as in the case of the Au/CeO_2 catalyst. This allows claim for synergy between both supports in such a way that the montmorillonite phase hinders particle growths either by influencing the nucleation behavior of gold or by increasing the number of nucleation sites and raising the overall dispersion.

3.1. 4-NP reduction

Fig. 3 reports the evolution of the UV-vis spectra with time for the catalytic reduction of 4-NP to 4-AP at room temperature. Two absorption bands are clearly observed at 398 and 298 nm characteristic of the reactant (4-NP) and the 4-AP product, respectively.

The signal at 398 nm gradually decreases, while the band ascribed to 4-AP merges. The reaction carried out in the presence of the bare supports, either CeO_2 or Mt, shows no activity, which suggests that gold is directly involved in 4-AP formation. However, the support plays a fundamental role in the activity when gold is present; the reaction reaches completion after 14 min when Au–Mt catalyst is used (Fig. 3A), decreasing the completion time for Au/CeO_2

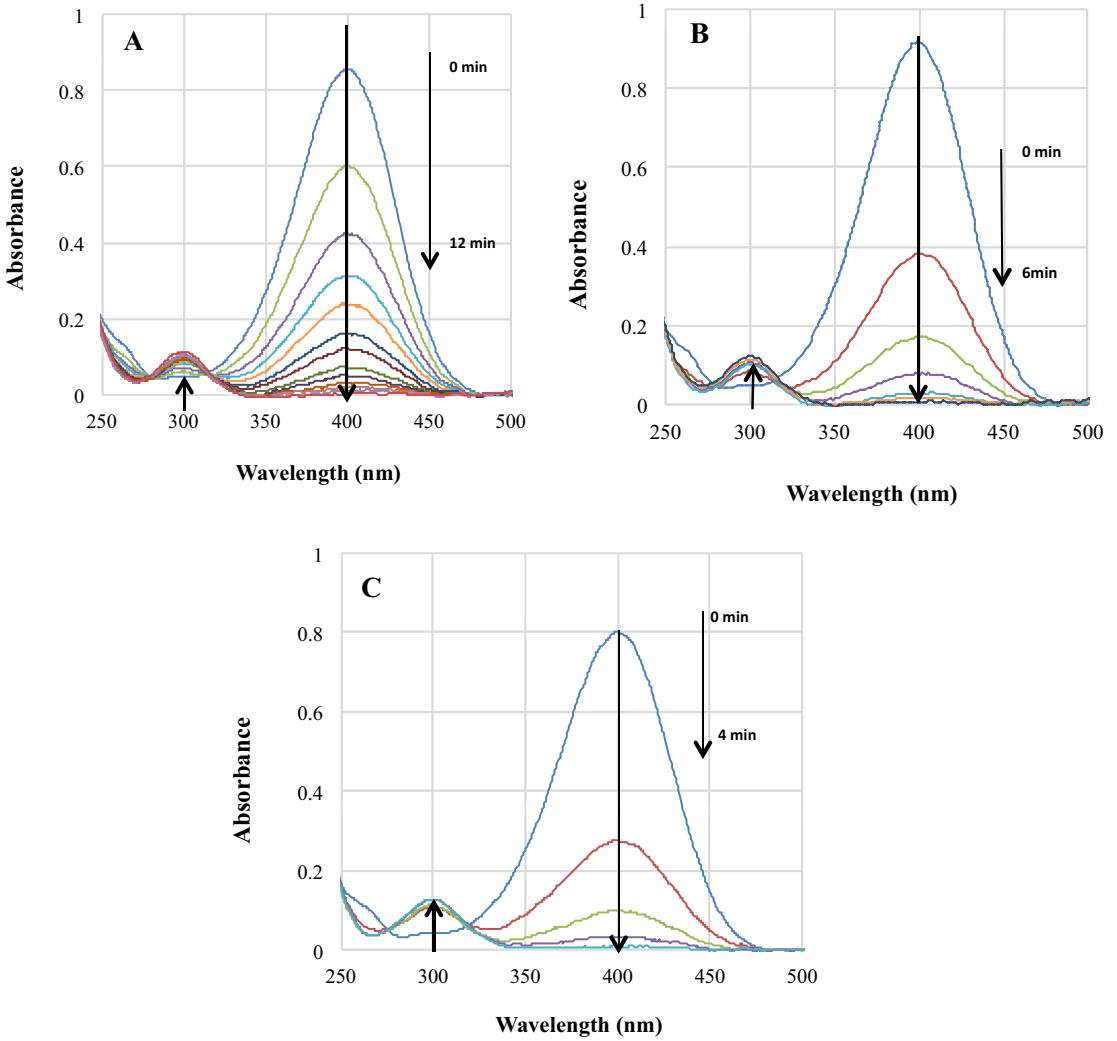

Fig. 3. UV-vis absorption spectra during the reaction over (A) Au–Mt, (B) Au/CeO_2, and (C) $Au–Mt/CeO_2$.

Table 2
Apparent rate constants for prepared samples and comparison with reported data.

Catalyst	Au size, nm	k_{app}*10^{-2} s^{-1}	k_{norm}, s^{-1}·mmol Au^{-1}	Ref
Au–Mt	5.5	0.65	9.6	This work
Au/CeO_2	5.6	1.41	11.6	This work
$Au–Mt/CeO_2$	4	1.82	24.1	This work
AuNPs@CeO_2-NTs	5	0.22	14	[40]
Au/Al_2O_3	3.4	1.10	22	[41]
Au/ILs/PpyNTs	5.7	0.58	–	[20]
AuNP(1.6 nm)_Me-Im@SBA-15	1.6	0.17	56.8	[30]
K10_A@Au	4–5	0.15	630	[42]

(Fig. 3B) and $Au–Mt/CeO_2$ catalyst (Fig. 3C) to 6 and 4 min, respectively.

A good linear correlation is observed by plotting the $\ln(A_t/A_0)$ versus time, where A_0 and A_t are the absorbances for 4-NP in the reaction mixture for the initial concentration (C_0) and the remaining concentration as a function of time (C_i), respectively. The apparent reaction rate constants calculated this way are shown in Table 2. To best compare the obtained results, these rate constants have been normalized by the amount of loaded gold (k_{norm}, s^{-1}·mmol Au^{-1}) and literature results (Table 2).

As a general trend, decreasing the particle increases size the rate constant. This points to the key role of gold particle size in the reaction. Thus, the lower the particle size, the higher the apparent rate constant. Density functional theory (DFT) calculations have shown that the binding energy of the BH_4 anion on Au(111) is 0.41 eV [43], while on Au(100), it has been reported to be −2.57 eV [44]. Further dissociation is a favorable downhill process whatever the

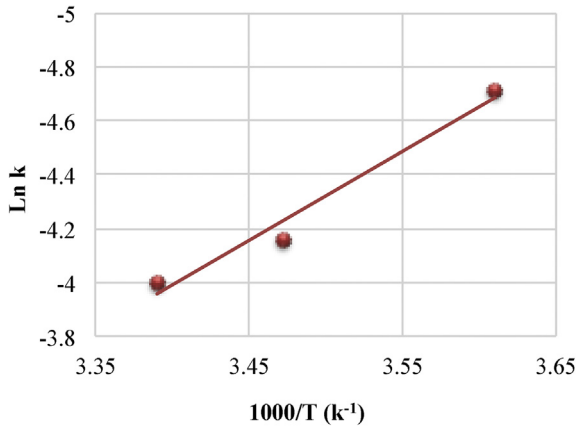

Fig. 4. Arrhenius plot for the reduction of 4-NP on the Au/CeO_2 catalyst. 4-NP, 4-nitrophenol.

face exposed by gold nanoparticles. These data suggest that the catalytic reduction of 4-NP by BH_4 anions is a structure-sensitive reaction, and hence, the particle size should affect the catalytic performances. As the relative Au(100)-to-Au(111) ratio increases on decreasing particle size, the smaller the particle size, the stronger and easier the adsorption of BH_4 anions and the higher the specific activity of the gold catalyst.

The mechanism of the catalytic reaction has been modeled by four successive steps. First, BH_4 anion adsorption occurs on the gold surface and the anions further dissociate, forming surface-hydrogen species. This hydrogen surface species reacts either with adsorbed 4-NP (Langmuir-Hinshelwood [LH] model) or with 4-NP molecules diffusing from solution to the surface (Eley-Rideal [ER] model). Considering that diffusion, adsorption and desorption processes are reversible and fast, and the reduction of 4-NP becomes the rate-determining step. Wunder et al. [45,46] proposed an LH mechanism for this reaction, whereas an ER one is more recently proposed by Suchomel et al. [47] who also observed a specific activity increase on decreasing the particle size. Shin et al. [48] also support the LH mechanism by claiming that the reduction process is assured by the release of electrons from the BH_4 anion (donor) to 4-NP (acceptor) on the metal surface.

However, by taking into consideration the Au–Mt and Au/CeO_2 catalysts that present the same average particle size, other factors may be considered. Similar rate constants should be expected for these two samples if particle size were to determine the specific activity alone. Therefore, the role of the support cannot be underestimated because both BH_4 anions and 4-NP may interact with the support surface. 4-NP adsorbs on the ceria surface, with the adsorption capacity depending on the number of surface oxygen vacancies. Guzman et al. [49] have shown that up to 30 mg/g of 4-NP may adsorb on ceria, considering the surface area of the ceria-containing catalysts (Table 1). This adsorption capacity accounts for up to one 4-NP molecule per square nanometer of the ceria surface. Besides adsorption, surface electronic effects could arise at the metal/support interface. The role of the Au-support interface has been previously highlighted [50]. The molecule to react interacts at the same time with both the metal and the support, allowing the insertion of H atoms on the nitro group. The apparent activation energy is estimated by varying the reaction temperature in the 277–295 K temperature range (Fig. 4). The obtained value (~27 kJ mol^{-1}) is considerably lower than those previously reported in the literature. The apparent activation energies for polymer-supported (polymethyl methacrylate PMMA) gold catalysts is 38 kJ mol^{-1} for Au-PMMA [51] and 34 kJ mol^{-1} for unsupported hollow gold nanoparticles [52]; moreover, for unsupported bimetallic Au–Ag nanoparticles, the apparent activation energy is even much higher (56 kJ mol^{-1}) [53]. These data may suggest that the support lowers the activation energy of the reaction probably by stabilizing the reaction intermediate at the metal-support interface.

Reuse experiments were carried out in five successive runs to study the deactivation of the $Au–Mt/CeO_2$ catalyst. Between runs, the catalyst was recovered by filtration and reused under the same reaction conditions without any further pretreatment. Fig. 5 plots the observed conversion after 4 min of reaction as a function of the reuse cycle.

For the first three cycles, the catalyst performances remain unaltered. However, after the third cycle, the activity starts to slowly decrease but keeping 80% of the initial 4-NP conversion after the fifth run.

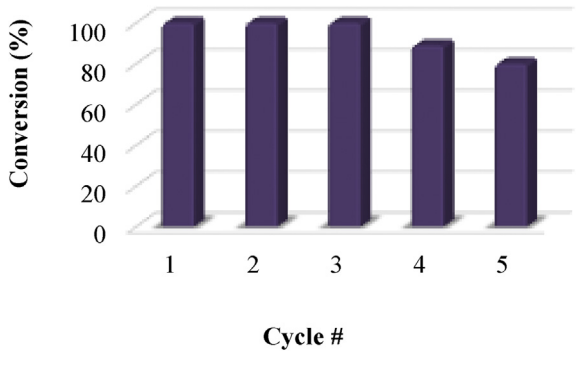

Fig. 5. Reuse cycles of the $Au–Mt/CeO_2$.

4. Conclusions

A series of montmorillonite-containing catalysts were prepared and studied for the catalytic reduction of 4-NP by $NaBH_4$. Montmorillonite stabilizes gold nanoparticles, but the initial clay structure is dramatically altered by the synthesis procedure, resulting in a drastic decrease of the specific surface area and low catalytic activity for the 4-NP reduction. However, the use of a mineral support (cerium oxide) in conjunction with montmorillonite results in more disperse metal particles, while keeping the surface area of the ceria support and leading to a more active catalyst. Synergy between montmorillonite and ceria is postulated in such a way that the montmorillonite phase hinders particle growth either by influencing the nucleation behavior of gold or by increasing the number of nucleation

sites and raising the overall dispersion. The role of the ceria support, on the other hand, may be associated with the 4-NP adsorption at the ceria-gold interface, stabilizing the reaction intermediate and hence lowering the activation barrier for the reduction of 4-NP to 4-AP.

References

[1] M. Nemanashi, R. Meijboom, J. Colloid Interface Sci. 389 (2013) 260–267.
[2] J.-R. Chiou, B.-H. Lai, K.-C. Hsu, D.-H. Chen, J. Hazard Mater. 248–249 (2013) 394–400.
[3] B. Zhao, G. Mele, I. Pio, J. Li, L. Palmisano, G. Vasapollo, J. Hazard Mater. 176 (2010) 569–574.
[4] Y.S. Seo, E.-Y. Ahn, J. Park, T.Y. Kim, J.E. Hong, K. Kim, et al., Nanoscale Res. Lett. 12 (2017) 7.
[5] Environmental Protection Agency: Washington DC, EPA, Nitrophenols, Ambient Water Quality Criteria, 1978.
[6] O.A. O'Connor, L.Y. Young, Environ. Toxicol. Chem. 8 (1989) 853–862.
[7] M.S. Dieckmann, K.A. Gray, Water Res. 39 (1996) 1169–1183.
[8] E. Marais, T. Nyokong, J. Hazard Mater. 152 (2008) 293–301.
[9] L.L. Bo, Y.B. Zhang, X. Quan, B. Zhao, J. Hazard Mater. 153 (2008) 1201–1206.
[10] M.A. Oturan, J. Peiroten, P. Chartrin, A.J. Acher, Environ. Sci. Technol. 34 (2000) 3474–3479.
[11] P. Cañizares, C. Sáez, J. Lobato, M.A. Rodrigo, Ind. Eng. Chem. Res. 43 (2004) 1944–1951.
[12] C.V. Rode, M.J. Vaidya, R.V. Chaudhari, Org. Process Res. Dev. 3 (1999) 465–470.
[13] M.J. Vaidya, S.M. Kulkarni, R.V. Chaudhari, Org. Process Res. Dev. 7 (2003) 202–208.
[14] Y. Du, H. Chen, R. Chen, N. Xu, Appl. Catal. Gen. 277 (2004) 259–264.
[15] Y.-C. Chang, D.-H. Chen, J. Hazard Mater. 165 (2009) 664–669.
[16] M. Karlíková, L. Kvítek, R. Prucek, A. Panáček, J. Filip, J. Pechoušek, et al., Phys. Procedia 44 (2003) 231–237.
[17] A.K. Ilunga, R. Meijboom, Appl. Catal. B Environ. 203 (2017) 505–514.
[18] W. Ye, J. Yu, Y. Zhou, D. Gao, D. Wang, C. Wang, et al., Appl. Catal. B Environ. 181 (2016) 371–378.
[19] Z. Zhang, C. Shao, P. Zou, P. Zhang, M. Zhang, J. Mu, et al., Chem. Commun. 47 (2011) 3906–3908.
[20] L. Qiu, Y. Peng, B. Liu, B. Lin, Y. Peng, M.J. Malik, et al., Appl. Catal. Gen. 413–414 (2012) 230–237.
[21] N. Anand, P. Ramudu, K.H.P. Reddy, K.S.R. Rao, B. Jagadeesh, V.S.P. Babu, et al., Appl. Catal. Gen. 454 (2013) 119–126.
[22] F.H. Lin, R.A. Doong, Appl. Catal. Gen. 486 (2014) 32–41.
[23] Y. Dai, P. Yu, X. Zhang, R. Zhuo, J. Catal. 337 (2016) 65–71.
[24] H.S. Schrekker, M.A. Gelesky, M.P. Stracke, C.M.L. Schrekker, G. Machado, S.R. Teixeira, et al., J. Colloid Interface Sci. 316 (2007) 189–195.
[25] K. Shang, Y. Geng, X. Xu, C. Wang, Y.I. Lee, J. Hao, et al., Mater. Chem. Phys. 146 (2014) 88–98.
[26] W. Zhang, B. Liu, B. Zhang, G. Bian, Y. Qi, X. Yang, et al., Colloid. Surf. Physicochem. Eng. Asp. 466 (2015) 210–218.
[27] R. Ciganda, N. Li, C. Deraedt, S. Gatard, P. Zhao, L. Salmon, et al., Chem. Commun. 50 (2014) 10126–10129.
[28] S. Ivanova, V. Pitchon, Y. Zimmermann, C. Petit, Appl. Catal. Gen. 298 (2006) 57–64.
[29] R. Zanella, S. Giorgio, C.H. Shin, C.R. Henry, C. Louis, J. Catal. 222 (2004) 357–367.
[30] M. Boronat, A. Corma, F. Illas, J. Radilla, T. Ródenas, M.J. Sabater, J. Catal. 278 (2011) 50–58.
[31] H. Zhao, C.H. Zhou, L.M. Wu, J.Y. Lou, N. Li, H.M. Yang, et al., Appl. Clay Sci. 74 (2013) 154–162.
[32] S. Letaief, S. Grant, C. Detellier, Appl. Clay Sci. 53 (2011) 236–243.
[33] L. Zhu, S. Letaief, Y. Liu, F. Gervais, C. Detellier, Appl. Clay Sci. 43 (2009) 439–446.
[34] A. Álvarez, S. Moreno, R. Molina, S. Ivanova, M.A. Centeno, J.A. Odriozola, Appl. Clay Sci. 69 (2012) 22–29.
[35] S. Agarwal, J.N. Ganguli, J. Mol. Catal. A Chem. 372 (2013) 44–50.
[36] P.P. Sarmah, D.K. Dutta, Appl. Catal. Gen. 470 (2014) 355–360.
[37] E. Eren, B. Afsin, J. Hazard Mater. 151 (2008) 682–691.
[38] G.K. Sarma, S. Sen Gupta, K.G. Bhattacharyya, J. Environ. Manag. 171 (2016) 1–10.
[39] V.V. Krupskaya, S.V. Zakusin, E.A. Tyupina, O.V. Dorzhieva, A.P. Zhukhlistov, P.E. Belousov, et al., Minerals 7 (2017) 49.
[40] J. Zhang, G. Chen, M. Chaker, F. Rosei, D. Ma, Appl. Catal. B Environ. 132–133 (2013) 107–115.
[41] C. Lin, K. Tao, D. Hua, Z. Ma, S. Zhou, Molecules 18 (2013) 12609–12620.
[42] M. Rocha, P. Costa, C.A.D. Sousa, C. Pereira, J.E. Rodríguez-Borges, C. Freire, J. Catal. 361 (2018) 143–155.
[43] G. Rostamikia, R.J. Patel, I. Merino-Jimenez, M. Hickner, M.J. Janik, J. Phys. Chem. C 121 (2017) 52872–52881.
[44] L.H. Mendoza-Huizar, D.E.G. Rodríguez, C.H. Rios-Reyes, A. Alatorre-Ordaz, J. Mex. Chem. Soc. 56 (2012) 302–310.
[45] S. Wunder, F. Polzer, Y. Lu, Y. Mei, M. Ballauff, J. Phys. Chem. C 114 (2010) 8814–8820.
[46] S. Wunder, Y. Lu, M. Albrecht, M. Ballauff, ACS Catal. 1 (2011) 908–916.
[47] P. Suchomel, L. Kvitek, R. Prucek, A. Panacek, A. Halder, S. Vajda, et al., Sci. Rep. 8 (2018) 4589.
[48] K.S. Shin, J.Y. Choi, C.S. Park, H.J. Jang, K. Kim, Catal. Lett. 133 (2009) 1.
[49] M. Guzman, M. Estrada, S. Miridonov, A. Simakov, Microporous Mesoporous Mater. 278 (2019) 241–250.
[50] C. Megías-Sayago, K. Chakarova, A. Penkova, A. Lolli, S. Ivanova, S. Albonetti, et al., ACS Catal. 8 (2018) 11154–11164.
[51] K. Kuroda, T. Ishida, M. Haruta, J. Mol. Catal. A Chem. 298 (2009) 7–11.
[52] M. Guo, J. He, Y. Li, S. Ma, X. Sun, J. Hazard Mater. 310 (2016) 89–97.
[53] M.S. Holden, K.E. Nick, M. Hall, J.R. Milligan, Q. Chen, C.C. Perry, RSC Adv. 4 (2014) 52279–52288.